JOURNAL OF MATERIALS SCIENCE 35 (2000) 4329–4335

Oxygen vacancy concentration variation, diffusivity and thermo-chemical stability of $La_{0.2}Ba_{0.8}Co_{0.2}Fe_{0.8}O_{3-\delta}$ membranes

SHIGUANG LI**, WANQIN JIN, NANPING XU*, JUN SHI
Membrane Science and Technology Research Center, Nanjing University of Chemical Technology, Nanjing 210009, People's Republic of China
E-mail: npxu@dns.njuct.edu.cn

Perovskite type $La_{0.2}Ba_{0.8}Co_{0.2}Fe_{0.8}O_{3-\delta}$ (LBCF) powders were synthesized by modified citrate pyrolysis and LBCF membranes were prepared by isostatic pressing. The oxygen vacancy concentration variation of the LBCF powders becomes substantial above 973 K due to order-disorder transition. The unsteady-steady oxygen permeation flux of the LBCF membrane decreases with time and it takes about 40 min to get the steady state. In the temperature range of 1073–1223 K, the oxygen vacancy diffusivity of the LBCF membrane increases almost a magnitude and the increasing of oxygen permeation flux is mainly attributed to the increasing of oxygen vacancy diffusivity. An *in-situ* high-temperature X-ray diffraction was used to study the stability of the LBCF membrane, indicating that it has good thermochemical stability at elevated temperatures and low oxygen partial pressures.

1. Introduction

Over the past several years, A-site and B-site doped perovskite type oxides ($A_xA'_{1-x}B_yB'_{1-y}O_{3-\delta}$) have been investigated because of their mixed conducting behavior [1–7]. At elevated temperatures, these solid-solution compositions exhibit substantial ionic and electronic conductivity. Although the ionic conductivity in these materials frequently accounts for less than 1% of the overall electrical conductivity, the magnitude of that conductivity can be quite large relative to other oxygen ion conductors, such as yttria-stabilized zirconia (YSZ). This mixed conducting behavior results in a spontaneous flux of oxygen through dense sintered membranes when they are placed in an oxygen partial pressure gradient (feed: P'_{O_2}, permeate: P''_{O_2}) at elevated temperatures. Major potential applications of perovskite type dense membranes in chemical and petroleum industries are as membrane separator for oxygen from air [8–10] or as membrane reactors for partial oxidative reactions [11–15]. The dense membrane technology for air separation is economically attractive when integrated with a hot-turbine system [16]. Membrane reactor applications have focused on partial oxidation of hydrocarbons, e.g., upgrading natural gas to ethylene and ethane or syngas.

Most work in oxygen permeation through dense perovskite type membranes was focused on Sr doped $LaCo_xFe_{1-x}O_{3-\delta}$ oxides because of its high oxygen permeation fluxes. However, the substitution of Sr for the respective La decreases the high-temperature phase stability in low oxygen partial pressure environment. One of the typical examples is $SrCo_{0.8}Fe_{0.2}O_{3-\delta}$,which has a high reported oxygen permeation rate, 3.1 $cm^3/min \cdot cm^2$ (temperature: 1123 K, membrane thickness: 1 mm) [1], but has both an abrupt first-order phase transition at around 1063 K [17] and a susceptibility to reduction in the reducing atmospheres [18].

In this work we mainly concentrated on a Ba doped material on the A-site, i.e., $La_{0.2}Ba_{0.8}Co_{0.2}Fe_{0.8}O_{3-\delta}$ (LBCF) oxide. Oxygen vacancy concentration variation and diffusivity of the oxide were calculated by the TGA analysis and oxygen permeation flux study. Thermochemical stability of the LBCF membrane was investigated by an *in-situ* high-temperature X-ray diffraction (HTXRD) analysis.

2. Experimental procedure

2.1. Powder preparation and characterization

LBCF powders were prepared by the modified citrate pyrolysis method involving the following processes. Stoichiometric amounts of corresponding metal nitrates were dissolved in nitric acid (70%) with the acid to metal mole ratio of 2 : 1. Ammonia (30%) was then gradually dropped into the stirred nitrate solution to adjust the pH value of the solution to be 8–9. The gel-type homogeneous phase was then poured into a beaker and evaporated at around 473 K. Bubbles were formed vigorously and the solution became thicker. Cations

** *Current address*: Department of Chemical Engineering, University of Colorado, Boulder, CO 80309-0424, shiguang@colorado.edu
* Author to whom correspondence should be addressed.

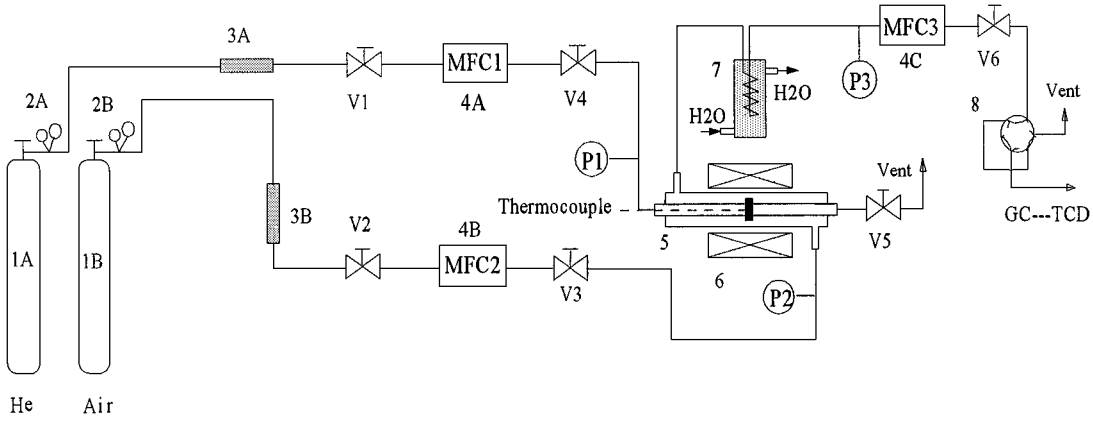

Figure 1 Apparatus used for oxygen permeation measurement. (1A, 1B) gas cylinders; (2A, 2B) gas regulators; (3A, 3B) purifying traps; (4A, 4B, 4C) mass flow controller; (5) permeation reactor; (6) furnace; (7) cooler; (8) six-way valves; (V1 ~ 6) flow control valves.

were mixed on a molecular level before a spontaneous combustion was initiated by the ammonium. The mouth of the beaker was covered with a fine sieve to prevent the loss of fine powders. To obtain homogeneity, particles were calcined for 5 h in air at 1303 K with typical heating and cooling rates of 2 K/min.

Thermogravimetric analysis (TGA, Model SDT2960) was performed on powder specimens from room temperature to 1573 K using heating and cooling rates of 5 K/min. Buoyancy corrections were performed using a platinum standard. The TGA measurements were performed in air and N_2 atmosphere (oxygen partial pressure of 1×10^{-3} atm).

2.2. Membrane preparation and characterization

The disk-shaped membranes were prepared by isostatic pressing. Detailed procedures for this membrane preparation had been given previously [19]. The membrane surface morphology was examined by high-resolution scanning electron microscopy (HR-SEM) (JEOL, JSM-6300). The densities of the sintered membranes were determined by the Archimedes method, using ethanol. These densities exceeded 90% of the theoretical in all cases.

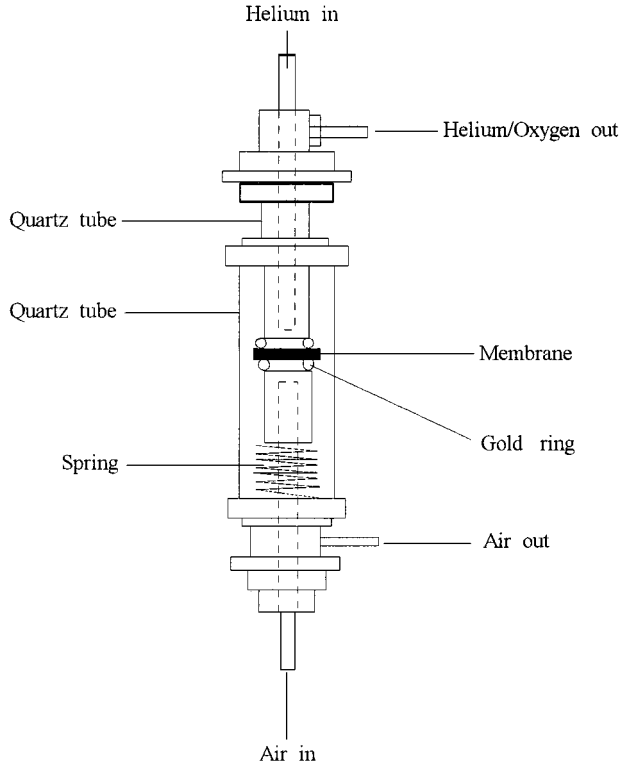

Figure 2 Oxygen separator.

2.3. Oxygen permeation flux measurement

The oxygen permeation rates through the membranes were measured on the apparatus shown in Fig. 1. The membrane separator is shown in Fig. 2. A sintered membrane disk was polished to the thickness of 2 mm and then mounted between two quartz tubes (ϕ 6 mm ID/12 mm OD). A quartz tube (ϕ 16 mm ID/19 mm OD) surrounding the two quartz tubes formed the shell side of the separator, which was surrounded by a tubular furnace. The temperature was measured by a type K thermocouple encased in an alumina tube. A microprocessor temperature controller (Model 708PA, Xiamen Yuguang Electronics Technology Research Institute, China) was used to control the temperature to within $\pm 1\,^{\circ}C$ of the set points. The flow rates of the inlet gases were controlled by mass flow controllers (Models D07-7A/ZM, Beijing Jianzhong Machine Factory, China). Air was introduced as the upstream gas of oxygen source. Helium as the sweeping gas for the permeating oxygen was fed to the downstream of the membrane. Both upstream and downstream gases were maintained at the atmospheric pressure. The effluent streams were analyzed by gas chromatography (Model Shimabzu GC-7A), which was equipped with a 2 m 5 A molecular sieve operated at 40 °C with H_2 as the carrier gas. The oxygen permeation flux through the membrane was calculated from the flow rates and the oxygen concentrations of the effluents.

2.4. Thermochemical stability study

The thermochemical stability of the resulting membranes was determined by an *in-situ* high-temperature X-ray diffraction (HTXRD) analysis using Cu K_α radiation (PAD X, Scintag Inc.). Each sample was tested at several temperatures in oxygen-rich atmosphere

(in air) and oxygen-lean atmosphere (in argon) using a Pt holder. The heating rate was 4 K/min, and the sample was stabilized at every temperature for 1 h. A range of diffraction angles from the degree 20° to 90° was used. Data collection was accomplished using DMSNT software (Scintag inc., Cupertino, CA) and data analysis was undertaken using Jade software (Materials Data Inc., Livermore, CA).

3. Results and discussion

3.1. SEM results

Fig. 3 shows surface and cross-section SEM photographs of the LBCF membrane. Grain boundaries were visible in the Figures. Closed porosity can be seen in the surface photo. Nitrogen permeation rate measurement confirmed that open porosity did not exist.

3.2. Oxygen vacancy concentration variation

Fig. 4 shows TGA results of LBCF powders in air and N_2 atmosphere (oxygen partial pressure of 1×10^{-3} atm). From the Figure, deviation from ideal oxygen stoichiometry (δ) and oxygen vacancy concentration variation (ΔC_v) of the LBCF powders at different temperature can be obtained, assuming that δ is the same at room temperature in air and N_2 atmosphere. ΔC_v is related to δ by:

$$\Delta C_v = \frac{\delta_{N_2} - \delta_{air}}{V_m} \tag{1}$$

where δ_{N_2} and δ_{air} are respectively δ of the oxide at air and N_2 atmosphere. V_m is the molar volume of the oxide. According to the TGA results, $\delta_{N_2} - \delta_{air}$ can be given by:

$$\delta_{N_2} - \delta_{air} \approx \frac{M}{16}\left(\Delta W_{N_2}\% - \Delta W_{air}\%\right) \tag{2}$$

where $\Delta W_{N_2}\%$, $\Delta W_{air}\%$ are respectively weight change percents of the oxide in N_2 and air atmosphere. M is the molar mass (g/mol) of the LBCF oxide.

Substitution of $V_m = \frac{M}{\rho}$ and Equation 2 into Equation 1 yields the oxygen vacancy concentration,

$$\Delta C_v \approx \frac{\rho}{16}\left(\Delta W_{N_2}\% - \Delta W_{air}\%\right) \tag{3}$$

For the LBCF oxide, the theoretical density (g/cm^3), ρ, can be obtained from the TGA and HTXRD results. As will be stated in Section 3.4, the weighth decreases and lattice parameter increases with the increasing temperature. Therefore, the theoretical density is a function of temperature. The values can be calculated to be 6.91 and 6.13 g/cm^3 at the temperature of 303 and 1223 K, respectively.

Fig. 5 shows the calculated oxygen vacancy concentration variations of LBCF powders in air and N_2 atmosphere as a function of temperature. As shown, when the temperature is less than 1073 K, the oxygen vacancy concentration variations increase with the increasing temperature and become substantial above 973 K due to order-disorder transition of the oxygen vacancy [14, 17]. When the temperature is higher than 1073 K, the oxygen vacancy concentration variations are high and almost keep unchanged with the changing temperature.

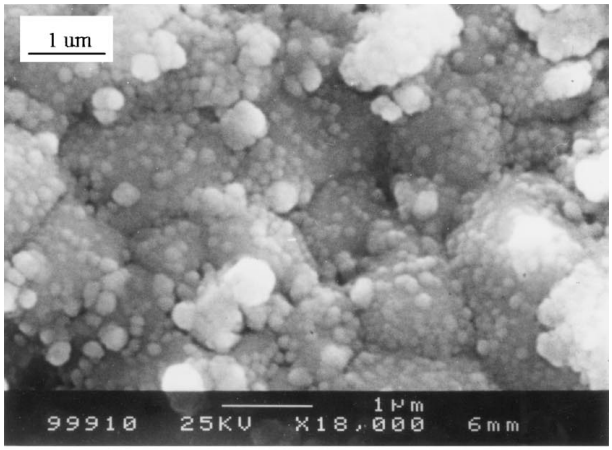

(a)

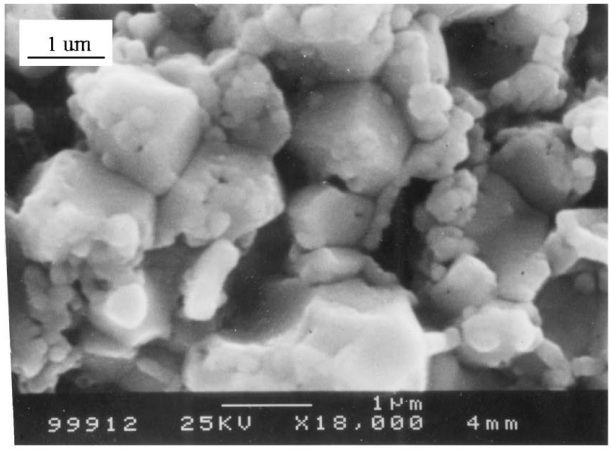

(b)

Figure 3 SEM photographs of the LBCF membrane. (a) surface; (b) cross-section.

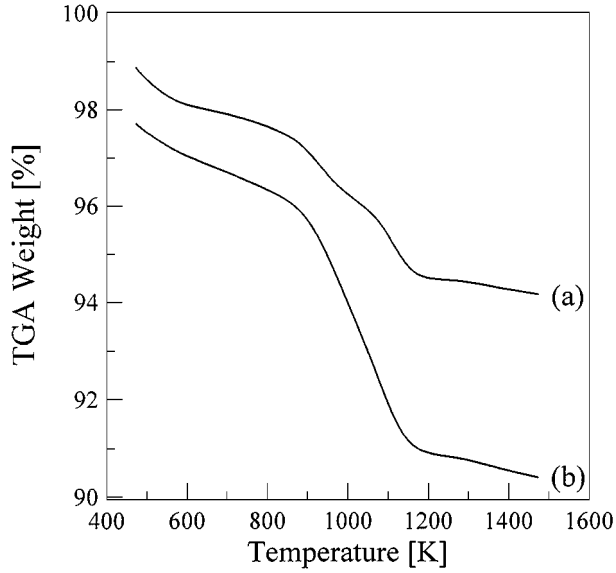

Figure 4 TGA results of the LBCF powders: (a) in air; (b) in N_2.

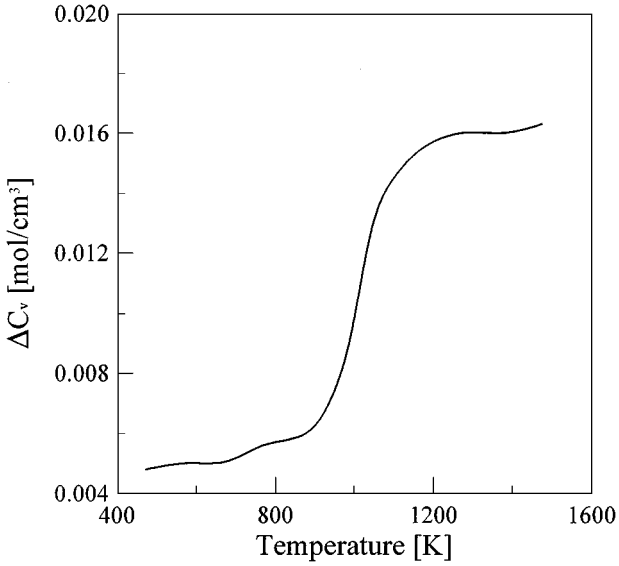

Figure 5 Temperature dependence of the oxygen vacancy concentration variation of the LBCF membrane.

3.3. Oxygen permeation flux and oxygen vacancy diffusivity

Fig. 6 shows oxygen permeation flux of the LBCF membrane as a function of time after the downstream gas was shifted from air to helium (upstream was air). The oxygen permeation flux, starting at a much higher value, decreases with time and eventually levels off. By a simple quantitative analysis on the transient permeation phenomenon using an oxygen vacancy concentration transfer model, the oxygen permeation flux J_{O_2} can be obtained:

$$J_{O_2} = \frac{D_v(C_v'' - C_v')}{2L}\left[1 + \sum_1^{\infty} 2\,e^{-D_v n^2 \pi^2 t/L^2}\right] \quad (4)$$

where D_v is the oxygen vacancy diffusivity, C_v'', C_v' are the downstream and upstream oxygen vacancy concentrations, respectively. L is the membrane thickness, and t is the time.

Equation 4 indicates that the measured oxygen flux includes two parts: the time-independent, steady-state contribution; and a time-dependent contribution due to the loss of the oxygen in the membrane material. When $t = 0$, $J_{O_2} \to \infty$. Thus, initially very large oxygen permeation flux could be observed. The oxygen permeation flux decreases with time, with the rate depending on the oxygen vacancy diffusivity and membrane thickness, as shown by Equation 4. Equation 4 also shows that when $t \to \infty$, the oxygen permeation flux at steady state can be obtained:

$$J_{O_2} = \frac{D_v(C_v'' - C_v')}{2L} \quad (5)$$

The transient period toward steady-state oxygen permeation of La-Sr-Co-Fe membranes were investigated by several groups [6, 14, 17, 19]. In this study, the transient time of LBCF membrane was found to be about 40 min. The following oxygen fluxes were obtained in the steady-state, so Equation 5 can be used to describe the oxygen permeation flux.

Fig. 7 shows oxygen permeation fluxes through the LBCF membrane at different temperatures ($P'_{O_2} = 0.21$ atm, $P''_{O_2} = 1 \times 10^{-3}$ atm). As shown, the flux increase with the increasing temperature and become substantial above 1073 K, which is in agreement with the result of ΔC_v.

Fig. 8 gives the calculated oxygen vacancy diffusivity of the LBCF membrane as a function of temperature ($P'_{O_2} = 0.21$ atm, $P''_{O_2} = 1 \times 10^{-3}$ atm) using Equation 5. As shown, the oxygen vacancy diffusivity increases with the increasing temperature and there is almost a magnitude increase from 1073 to 1223 K. Therefore the increasing oxygen permeation flux of the LBCF membrane can be explained as follows. When the operation temperature is less than 1073 K, both oxygen vacancy concentration variation and diffusivity enlarge the oxygen permeation flux. When the operation temperature is higher than 1073 K, since the oxygen vacancy concentration variation almost keeps unchanged, the increasing of oxygen permeation flux

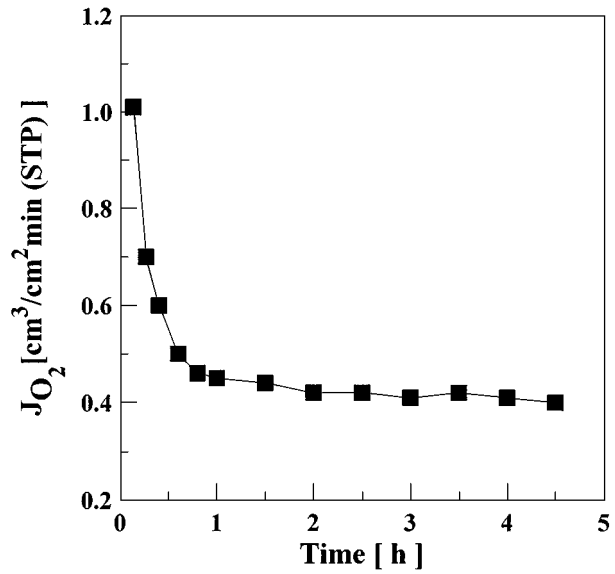

Figure 6 Time dependence of the oxygen permeation flux of the LBCF membrane.

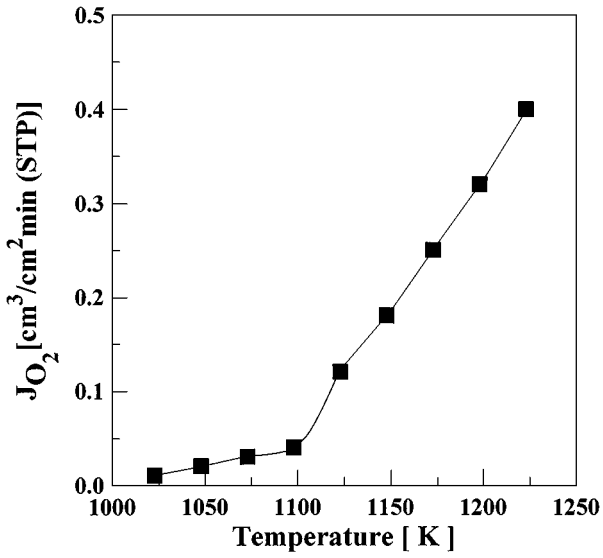

Figure 7 Temperature dependence of the oxygen permeation flux of the LBCF membrane ($P'_{O_2} = 0.21$ atm, $P''_{O_2} = 1 \times 10^{-3}$ atm).

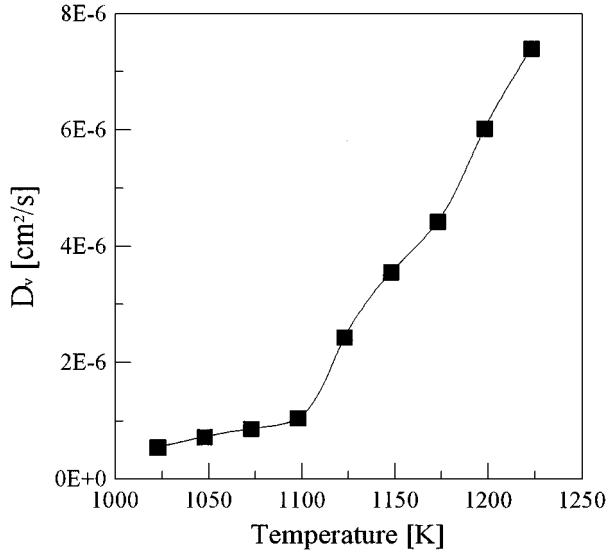

Figure 8 Temperature dependence of the oxygen vacancy diffusivity of the LBCF membrane ($P'_{O_2} = 0.21$ atm, $P''_{O_2} = 1 \times 10^{-3}$ atm).

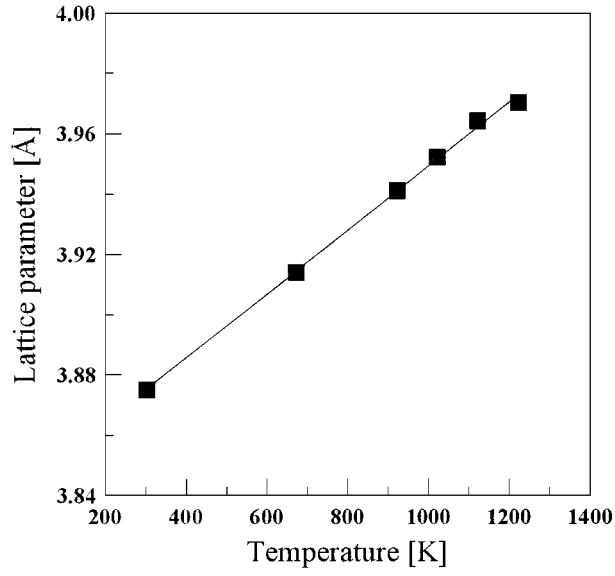

Figure 10 Temperature dependence of lattice parameter of the LBCF membrane.

mainly attributed to the increasing of oxygen vacancy diffusivity.

3.4. Thermochemical stability

Fig. 9 shows X-ray diffraction patterns of LBCF membranes at various temperatures in air. As shown, The LBCF membrane is stable at temperatures up to 923 K in oxygen-rich atmosphere (air). However, at the temperatures higher than 923 K, new peaks appeared near the characteristic peak (P(200) and P (220)) and the characteristic peak was not obvious, which was due to the thermal expansion of Pt holder. Eliminating the influence of the Pt holder, The LBCF membrane is phase stable up to 1223 K in air atmosphere. Crystallographic lattice parameters were obtained by X-ray powder diffraction at high temperatures shown in Fig. 10. As can be seen, lattice parameter of the LBCF oxide increases about 2.3% (3.88 Å to 3.97 Å) as the temperature changes from 303 to 1223 K.

Fig. 11 shows X-ray diffraction patterns of LBCF membranes at various temperatures in argon (oxygen partial pressure of 1×10^{-3} atm). As shown, the XRD patterns and peak broadness of LBCF membrane after exposure to Ar at various temperatures remain essentially same. No new phases are formed in this membrane after these treatments. This shows that LBCF membrane is more stable at high temperature and low oxygen partial pressure. During the oxygen permeation measurement, the upstream and downstream

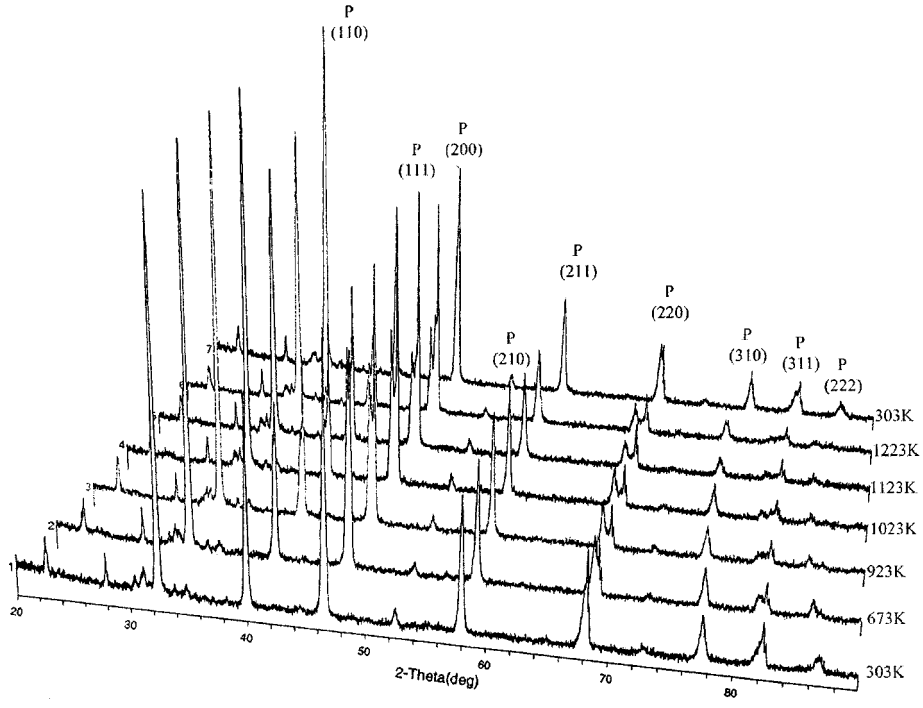

Figure 9 XRD patterns of LBCF membrane at various temperatures in air. (P) Perovskite.

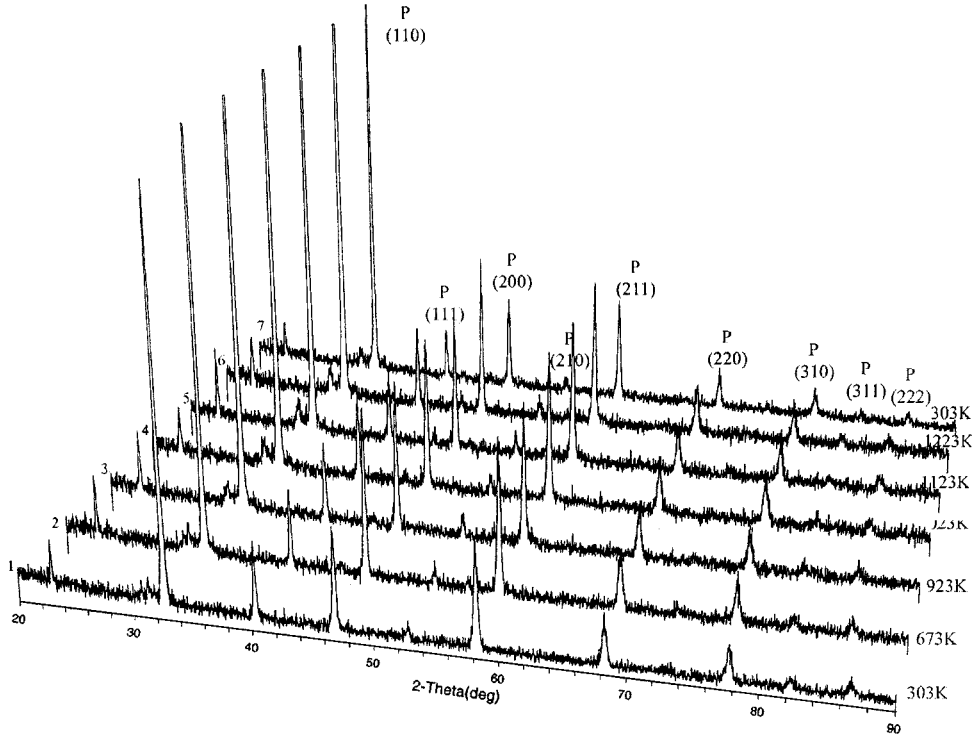

Figure 11 XRD patterns of LBCF membrane at various temperatures in argon. (P) Perovskite.

oxygen partial pressure were respectively about 0.21 and 1×10^{-3} atm), which was similar to the conditions of the *in-situ* HTXRD analysis in air and argon atmosphere. Therefore, The LBCF membrane is suitable for long-term oxygen separation.

4. Conclusion

The oxygen vacancy concentration variations of the prepared LBCF powders increase with the increasing temperature and become substantial above 973 K due to order-disorder transition. It keeps almost unchanged when the temperature is higher than 1073 K.

The unsteady-steady oxygen permeation flux of the LBCF membrane decreases with time and it takes about 40 min to get the steady-state. The steady-state fluxes increase with the increasing temperature and become substantial above 1073 K.

There is almost a magnitude increase of the oxygen vacancy diffusivity of the LBCF membrane from 1073 to 1223 K. In this temperature range, the increasing of oxygen permeation flux is mainly attributed to the increasing of oxygen vacancy diffusivity.

The LBCF membrane is very stable at temperatures up to 1223 K in oxygen-rich and low oxygen partial pressure atmosphere. Its good thermochemical stability indicates that it is suitable for long-term oxygen permeation operation.

Acknowledgements

This work is supported by the National Advanced Materials Committee of China (NAMCC, No. 715-006-0121) and the National Natural Science Foundation of China (NNSFC, No. 59789201). We also would like to acknowledge the support of the U. S. Department of Energy, Basic Energy Sciences, Division of Materials Sciences (USDOE/BES/DMS) on *in-situ* high temperature XRD analysis.

References

1. Y. TERAOKA, H. M. ZHANG, S. FURUKAWA and N. YAMAZOE, *Chem. Lett.* (1985) 1743.
2. MIZUSAKI, Y. MIMA, S. YAMAUCHI, K. FUKEI and H. TAGAWA, *J. Solid State Chem.* **80** (1989) 102.
3. T. H. LEE, Y. L. YANG, A. J. JACOBSON, B. ABELES and M. ZHOU, *Solid State Ionics* **100** (1997) 77.
4. T. M. GUR, A. BELZNER and R. A. HUGGINS, *J. Membr. Sci.* **75** (1992) 151.
5. V. V. KHARTON, E. N. NAUMOVICH and A. V. NIKOLAEV, *ibid.* **111** (1996) 149.
6. C. Y. TSAI, A. G. DIXON, Y. H. MA, W. R. MOSER and M. R. PASCUCCI, *J. Am. Ceram. Soc.* **81** (1998) 1437.
7. H. J. M. BOUWMEESTER and A. J. BURGGRAAF, in "Fundamentals of Inorganic Membrane Science and Technology," edited by A. J. Burggraaf and L. Cot (Elsevier Science B. V., Amsterdam, 1996) p. 435.
8. N. ITOH, T. KATO, K. UCHIDA and K. HARAYA, *J. Membr. Sci.* **92** (1994) 239.
9. J. E. TEN ELSHOF, H. J. M. BOUWMEESTER and H. VERWEIJ, *Solid State Ionics* **81** (1995) 97.
10. L. QIU, T. H. LEE, L.-M. LIU, Y. L. YANG and A. J. JACOBSON, *ibid.* **76** (1995) 321.
11. J. E. TEN ELSHOF, H. J. M. BOUWMEESTER and H. VERWEIJ, *Appl. Catal. A: General* **130** (1995) 195.
12. J. E. TEN ELSHOF, B. A. VAN HASSEL and H. J. M. BOUWMEESTER, *Catal. Today* **25** (1995) 397.
13. C. Y. TSAI, A. G. DIXON, W. R. MOSER and Y. H. MA, *AIChE J.* **43** (1997) 2741.
14. Y. ZENG, Y. S. LIN and S. L. SWARTZ, *J. Membr. Sci.* **150** (1998) 687.
15. S. J. XU and W. J. THOMSON, *Ind. Eng. Chem. Res.* **37** (1998) 1290.
16. R. M. THOROGOOD, R. SRINIVASAN, T. F. YEE and M. P. DRAKE, US Patent 5, 240, 480 (1993).

17. H. KRUIDHOF, H. J. M. BOUWMEESTER, R. H. E. V. DOOM and A. J. BURGGRAAF, *Solid State Ionics* **63–65** (1993) 816.
18. S. PEI, M. S. KLEEFISCH, T. P. KOBYLINSKI, K. FABER, C. A. UDOVICH, V. ZHANG-MCCOY, B. DABROWSKI, U. BALACHANDRAN, R. L. MIEVILLE and R. B. POEPPEL, *Catal. Lett.* **30** (1995) 201.
19. S. LI, W. JIN, P. HUANG, N. XU, J. SHI, Z.-C. H. MICHAEL, E. A. PAYZANT and Y. H. MA, *AIChE J.* **45** (1999) 276.

Received 5 August 1999
and accepted 7 March 2000